Thermal Decomposition Mechanism of Energetic Cyclo-pentazolate Salts $N_2H_5N_5$: A Deep Neural Network Potential Accelerated Molecular Dynamics Study

Jiao Zhang,[a, b] Caimu Wang,[a, b] Renyi Li,[c] Danyang Zhang,[a, b] Yaozhong Liu,[a, b] Guozhen Sheng, [a, b] Wei Guo,*[a, b]

[a] *Frontiers Science Center for High Energy Material (MOE), Beijing Institute of Technology, Beijing 100081, China*

[b] *Centre for Quantum Physics, Key Laboratory of Advanced Optoelectronic Quantum Architecture and Measurement (MOE), School of Physics, Beijing Institute of Technology, Beijing 100081, China*

[c] *Beijing Key Laboratory for Theory and Technology of Advanced Battery Materials, School of Materials Science and Engineering, Peking University, Beijing 100871, PR China*

Supplementary Information

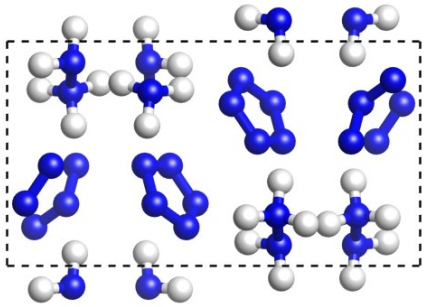

Figure S1. Unit cells of $N_2H_5N_5$ crystal. N and H atoms are colored blue gray and white, respectively. There are a total of 48 atoms within the cell.

The prefactor at training step t is given by:

$$p(t) = p^{\text{limit}}\left[1 - \frac{r_l(t)}{r_l^0}\right] + p^{\text{start}}\left[\frac{r_l(t)}{r_l^0}\right] \tag{1}$$

where p^{start} and p^{limit} are hyperparameters that give the prefactor at the first training step and the infinite training steps $r_l(t)$ and r_l^0 are the learning rate at training step t and training step 0 . $r_l(t)$ is defined as

$$r_l(t) = r_l^0 \times d_r^{t/d_s} \tag{2}$$

where d_r and d_s are the decay rate and decay steps, respectively.

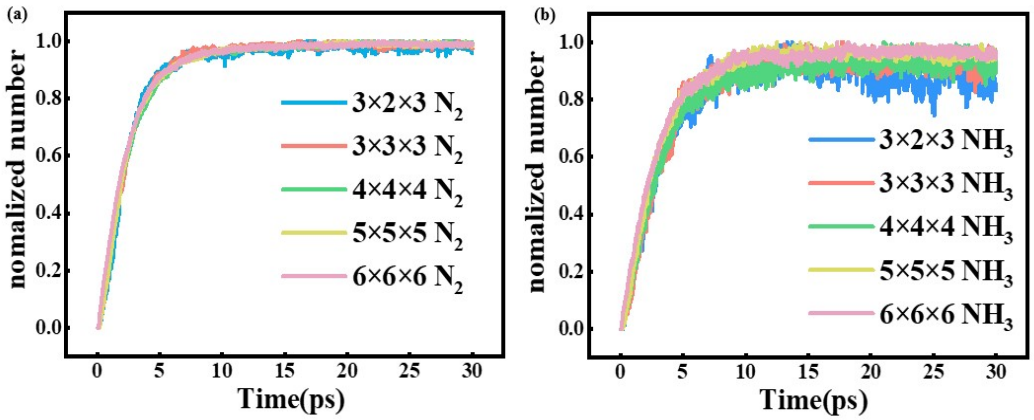

Figure S3. Numbers of N_2 (a), NH_3 (b) in the simulation of $N_2H_5N_5$ decomposition.

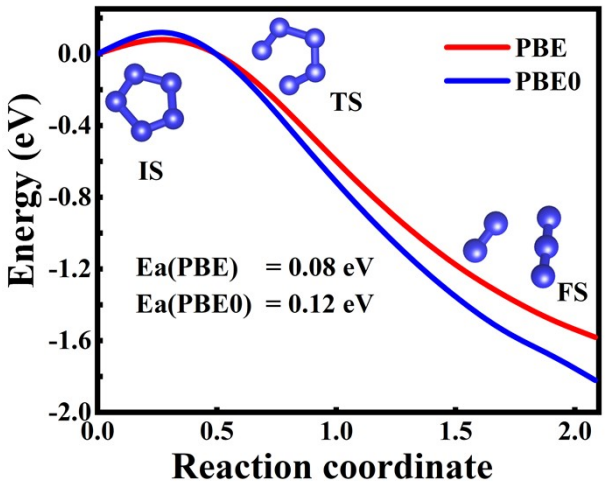

Figure S2 Reaction energy profiles for the N_5 ring-opening dissociation reaction. The minimum-energy pathway was obtained using the CI-NEB method at the PBE level. Single-point PBE0 energies were evaluated on selected structures along the PBE-

We systematically investigated the evolution of key chemical species during the

thermal decomposition of $N_2H_5N_5$. In Figure S3, we present a comparative analysis of

species evolution profiles obtained from ab initio molecular dynamics (AIMD) and

neural network potential molecular dynamics (NNP-MD) simulations. The NNP-MD

results demonstrate excellent agreement with AIMD data, capturing both the rapid

consumption of $N_2H_5N_5$ molecules and the formation of final products (predominantly

N_2 and NH_3). Importantly, for intermediate species such as HN_5 and N_2H_4, NNP-MD

successfully reproduces the evolution profiles observed in AIMD simulations,

confirming that our neural network potential (NNP) can accurately track transition-state structures during decomposition. Notably, while AIMD simulations exhibit significant fluctuations in species concentrations (Figure S3), NNP-MD maintains remarkably smooth evolution profiles despite simulating a system 18 times larger. This massive scale enhancement (thousands to millions of atoms) enables statistically robust analysis of macroscopic properties -a capability fundamentally beyond the reach of conventional AIMD methods. The successful extension to such large systems highlights the transformative potential of machine learning potentials in computational materials science.

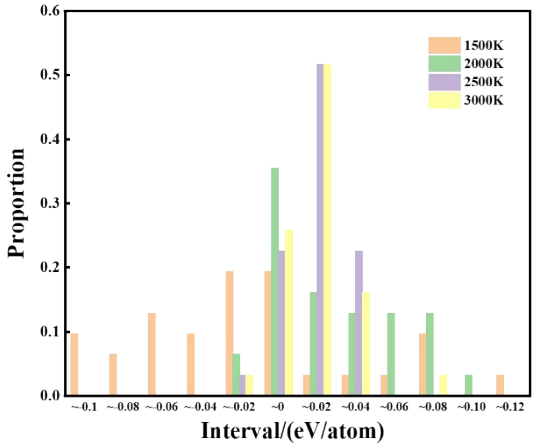

Figure S4. Error distribution of the energy of the partial structure at 1500 K, 2000 K, 2500 K, and 3000 K calculated by the NNP model and DFT.

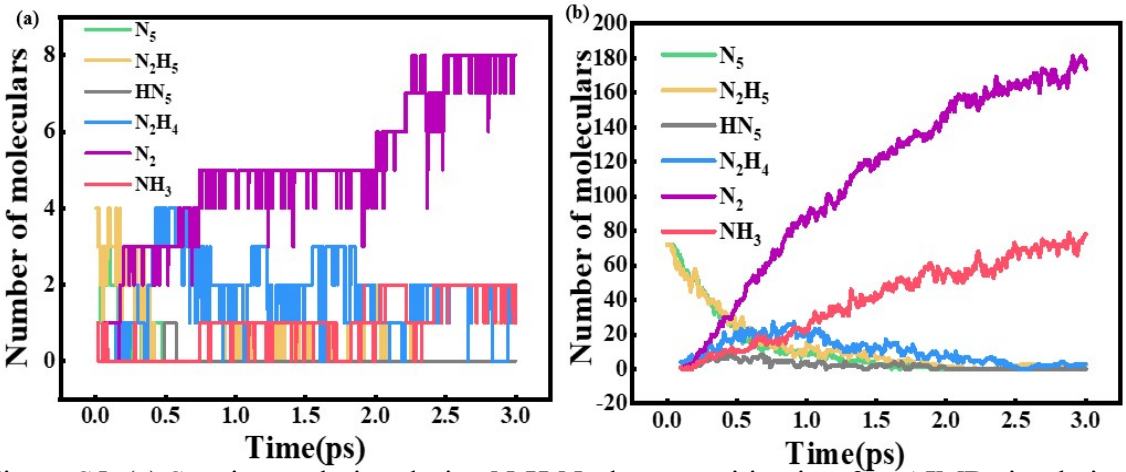

Figure S5. (a) Species evolution during $N_2H_5N_5$ decomposition in a 3ps AIMD simulation with four $N_2H_5N_5$ molecules (b) in a 3ps NNP-MD simulation with 72 $N_2H_5N_5$ molecules (3×2×3 supercells).

Table S1. Root mean square error and variance of partial structure energy at 1500 K, 2000 K, 2500 K, and 3000 K calculated by NNP model and DFT.

Temperature（K）	**Energy RMSE(eV/atom)**	**Energy Variance(eV)**
1500	0.06	7.21
2000	0.04	2.39
2500	0.01	0.45
3000	0.02	0.66

Table S2 net reaction frequencies of $N_2H_5^+$ within the initial 0–1.5ps

Time (ps)	Reactions	Net Frequencies
0-0.3 ps	$N_5 + N_2H_5 \rightarrow N_7H_5$	72
	$N_2H_5 + N_5 \rightarrow N_2H_4 + HN_5$	29
	$N_7H_5 \rightarrow N_2H_4 + HN_5$	17
	$2N_2H_5 \rightarrow N_4H_{10}$	13
	$N_4H_{10} + N_5 \rightarrow N_2H_5 + N_7H_5$	9
	$2N_2H_5 \rightarrow N_2H_4 + N_2H_6$	7
	$N_7H_6 \rightarrow N_2H_5 + HN_5$	7
	$N_2H_5 \rightarrow NH_2 + NH_3$	6
	$N_2H_6 + N_5 \rightarrow N_7H_6$	5
0.3-1.0 ps	$N_2H_5 + N_5 \rightarrow N_2H_4 + HN_5$	79
	$N_2H_5 \rightarrow NH_2 + NH_3$	27
	$N_2H_5 + N_5 \rightarrow N_7H_5$	25
	$N_2H_5 + N_3 \rightarrow N_5H_5$	22
	$N_2H_5 + N_3 \rightarrow N_2H_4 + N_3H$	20
	$N_7H_5 \rightarrow N_2H_4 + HN_5$	19
	$N_2H_6 \rightarrow 2NH_3$	18
	$N_5H_5 \rightarrow N_2H_4 + N_3H$	16
	$N_7H_4 \rightarrow N_2H_4 + N_5$	12
	$N_2H_5 + N_3H \rightarrow N_2H_4 + N_3H_2$	10
	$N_2H_5 + HN_5 \rightarrow N_2H_4 + N_5H_2$	9
	$N_5H_6 \rightarrow N_2H_4 + N_3H_2$	8
	$N_2H_4 + N_2H_6 \rightarrow 2N_2H_5$	7
	$N_4H_9 + N5 \rightarrow N_2H_4 + N_7H_5$	7

	$N_2H_5 + N_7H_5 \rightarrow N_9H_{10}$	6
	$N_2H_6 + N_5 \rightarrow N_2H_5 + HN_5$	6
	$N_4H_{10} \rightarrow N_2H_4 + N_2H_6$	6
	$N_{12}H_6 \rightarrow N_2H_5 + N5 + HN_5$	5
	$N_2H_3 + N_2H_5 \rightarrow 2N_2H_4$	5
	$N_2H_5 + N_3H \rightarrow N_5H_6$	5
	$N_2H_5 + N_7H_5 \rightarrow N_2H_4 + N_7H_6$	5
	$N_2H_6 + N_3 \rightarrow N_5H_6$	5
	$N_7H_5 \rightarrow NH_2 + NH_3 + N_5$	5
	$N_9H_9 \rightarrow N_2H_4 + N_7H_5$	5
1.0-1.5 ps	$N_2H_5 + N_3 \rightarrow N_2H_4 + N_3H$	19
	$N_2H_5 + N_5 \rightarrow N_2H_4 + HN_5$	18
	$N_7H_5 \rightarrow N_2H_4 + HN_5$	14
	$N_2H_5 \rightarrow NH_2 + NH_3$	12
	$N_2H_5 + N_3 \rightarrow N_5H_5$	9
	$NH_2 + N_2H_5 \rightarrow NH_3 + N_2H_4$	7
	$N_2H_5 + N_3H \rightarrow N_2H_4 + N_3H_2$	6
	$N_2H_5 + N_5 \rightarrow N_7H_5$	5
	$N_2H_6 \rightarrow 2NH_3$	5

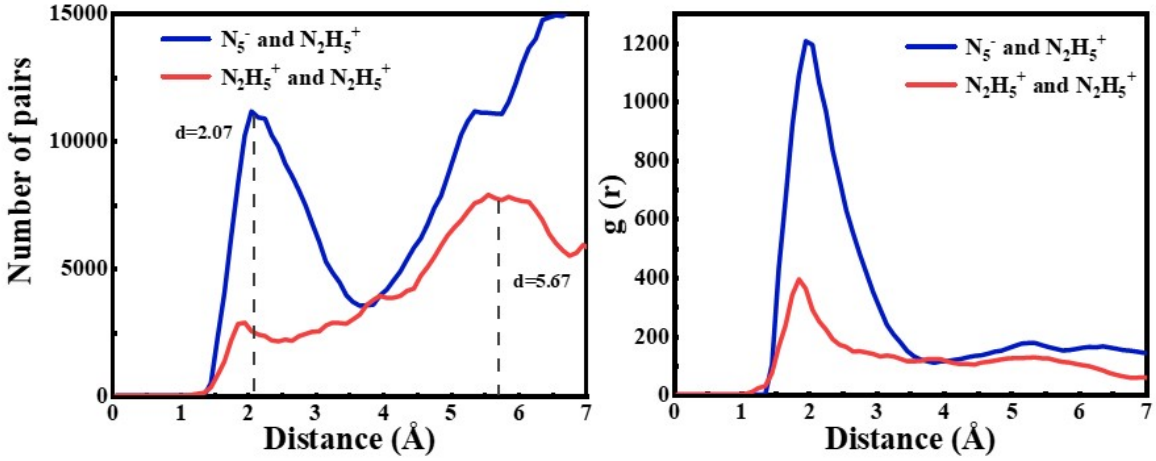

Figure S6. Pair distribution and population analysis of ionic interactions

(a) Distance-dependent number of particle pairs for N_5^- and $N_2H_5^+$ (blue) and $N_2H_5^+$ and $N_2H_5^+$ (red), accumulated over the molecular dynamics trajectory. The dashed vertical lines indicate the characteristic distances of the first and second coordination shells. A pronounced maximum at d ≈ 2.07 Å is observed for N_5^- and $N_2H_5^+$ pairs, indicating a strong preference for short-range association between oppositely charged species, whereas like-charged $N_2H_5^+$ and $N_2H_5^+$ pairs are significantly suppressed at short distances and redistributed to larger separations (d ≈ 5.67 Å).

(b) Radial distribution functions g(r) for the same pair types. The sharp first peak in g(r) for N_5^- and $N_2H_5^+$ confirms a strong short-range correlation beyond random distribution, while the weaker and broader peak for $N_2H_5^+$ and $N_2H_5^+$ reflects effective electrostatic repulsion. Together, these results demonstrate that electrostatic interactions dominate the local structural organization of the ionic species.

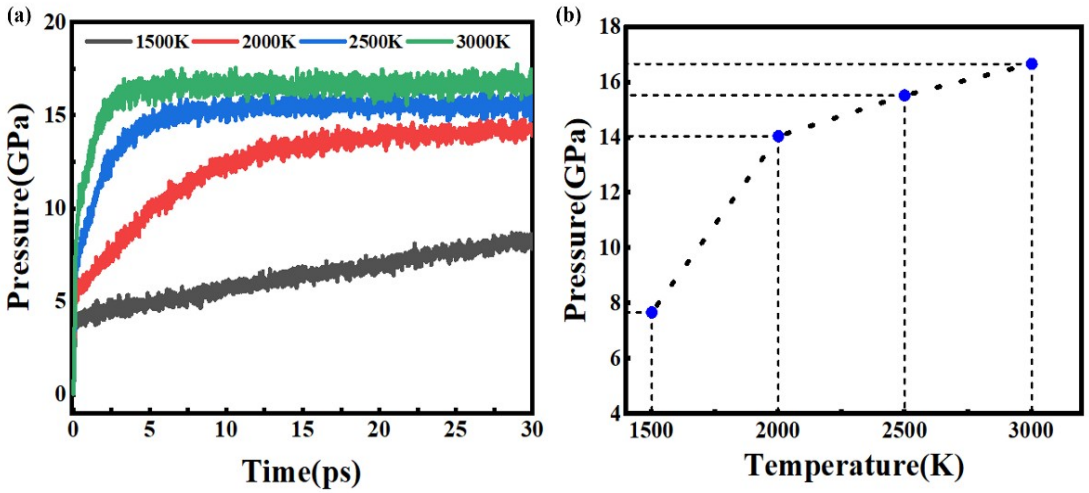

Figure S7. (a) Pressure evolution of $N_2H_5N_5$ crystal during decomposition at temperatures of 1500 K, 2000 K, 2500 K, and 3000 K. (b) Time-averaged pressure over the final 10 ps of simulation.

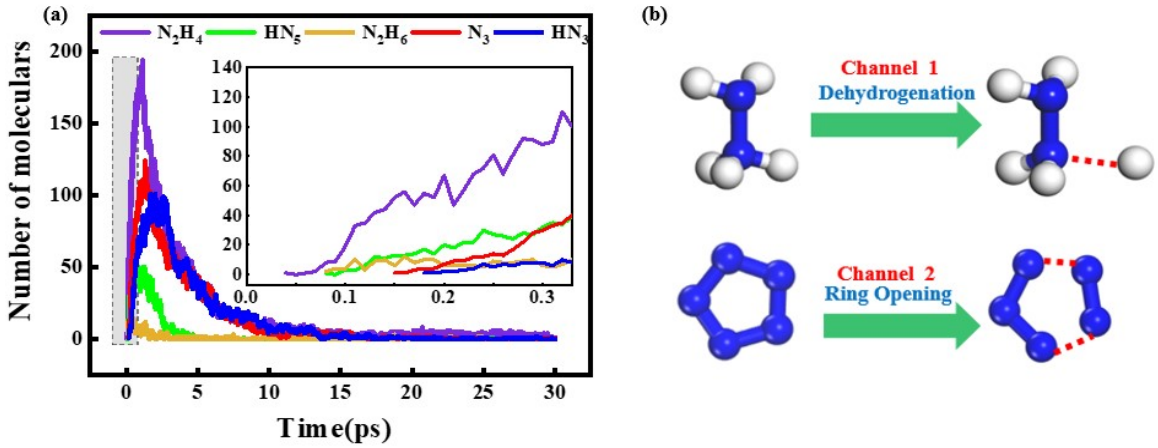

Figure S8. (a) Intermediate species evolution of $N_2H_5N_5$ crystal at 2500 K during the initial decomposition phase. (b) The initial decomposition channel of in $N_2H_5N_5$.

Figure S8 (a) shows the initial species evolution within the 30 ps. It can be seen that N_2H_4 is the earliest species, and N_2H_4 originates from the first initial dissociation channel in Figure S8 (b), namely cation dehydrogenation. It can be seen from the figure that the rate and quantity of N_2H_4 production are significantly greater than that of other species. Therefore, hydrogen-atom loss from the $N_2H_5^+$ constitutes the initial step in the thermal decomposition of $N_2H_5N_5$. Then a small amount of N_2H_6 appeared, which came from the transfer of protons between cations, and HN_5 began to appear in the system at about 0.05 ps, indicating that part of the shed hydrogen atoms trapped by N_5- formed HN_5. Then, azide ions (from channel 2) and HN_3 began to appear in the system, and the generation time of azide ions was earlier than that of HN_3. Azide ions came from the ring opening of N_5 ring, which indicated that the ring opening time of N_5 ring was earlier than that of HN_5 ring opening in the system. At the same time, HN_3 is produced immediately after N_3^-, indicating that N_3^- cannot exist stably in the system, but tend to combine with free hydrogen atoms.

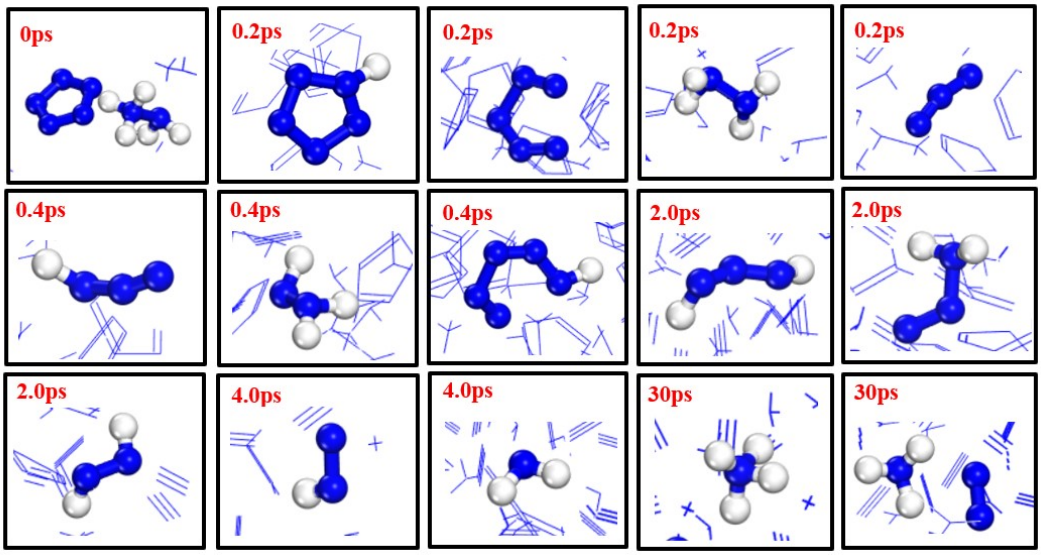

Figure S9. Snapshot sequence of key intermediates during the thermal decomposition of $N_2H_5N_5$. Blue represents nitrogen atoms and white represents hydrogen atoms.

Table S2. Calculation of reaction rate constants for $N_2H_5N_5$.

Temperature(K)	**k_{N5-} (1/ps)**	**k_{N2H5+} (1/ps)**
1500	0.0332	0.0404
2000	0.3087	0.2699
2500	0.9935	0.9630
3000	1.9569	1.9695

Table S3. Calculation of $N_2H_5N_5$'s rate constants based on N_2 production.

Temperature(K)	**k_{N2}(1/ps)**	**k_{N2_N5-} (1/ps)**	**k_{N2_N2H5+} (1/ps)**
1500	0.0518	0.05456	0.04132
2000	0.13479	0.14431	0.10951
2500	0.37445	0.4073	0.28646
3000	0.67817	0.75472	0.47643

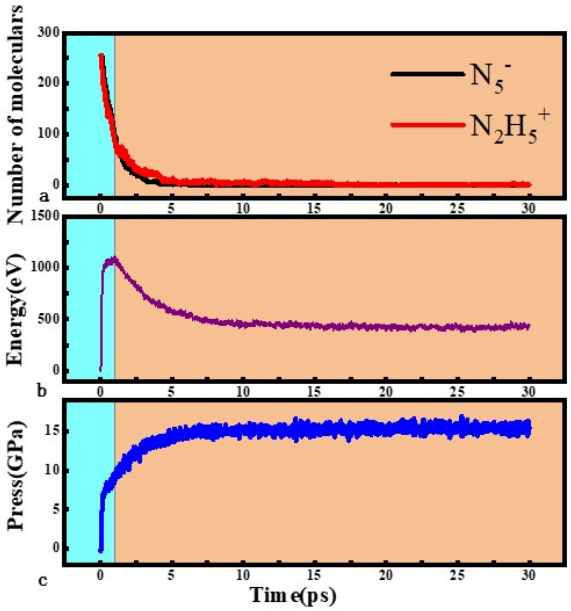

Figure S10. (a) The number (b)potential energy surface and(c) pressure evolution of the $N_2H_5N_5$ at 2500 K.

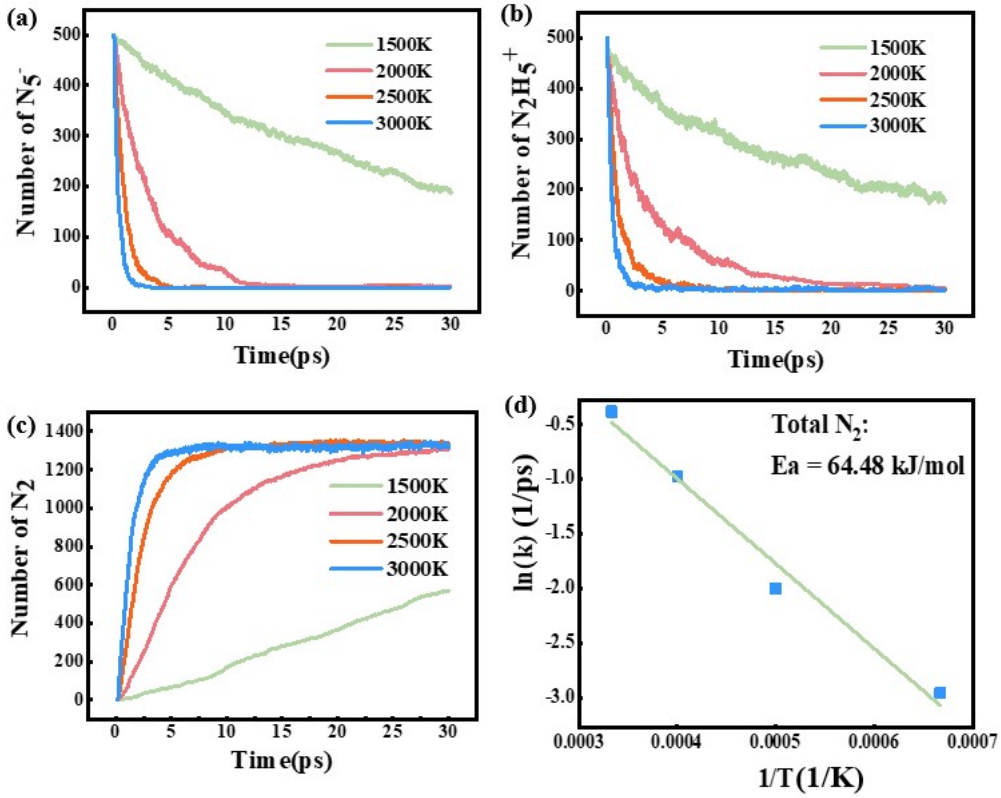

Figure S11. NNP predicted evolution of $N_2H_5N_5$ crystal under different temperatures. (a) N_5^- (b) $N_2H_5^+$. (c) NNP predicted evolution of N_2 molecule (d) The total reaction rate of N_2 in the system.